Molecular Biology Reports (2022) 49:12063–12075
https://doi.org/10.1007/s11033-022-08013-9

ORIGINAL ARTICLE

Mesenchymal stem cells encapsulation in chitosan and carboxymethyl chitosan hydrogels to enhance osteo-differentiation

Fereshteh Sharifi[1,2] · Maryam Hasani[3] · Seyed Mohammad Atyabi[4] · Baoqing Yu[5] · Behafarid Ghalandari[6] · Dejian Li[7] · Farnaz Ghorbani[7] · Shiva Irani[3] · Mohammadreza Gholami[8]

Received: 3 July 2022 / Accepted: 6 October 2022 / Published online: 31 October 2022

Abstract

Background Recently biomaterials utilized for designing scaffolds in tissue engineering are not cost-effective and eco-friendly. As a result, we design and develop biocompatible and bioactive hydrogels for osteo-tissue regeneration based on the natural polysaccharide chitosan. Three distinct hydrogel components were used for this.

Methods Hydrogels networks were created using chitosan 2% (CTS 2%), carboxymethyl chitosan 2% (CMC 2%), and 50:50 mixtures of CTS and CMC (CTS/CMC 50:50). Furthermore, scanning electron microscopy (SEM), Fourier transforms infrared spectroscopy (FTIR), degradation, and swelling behavior of design hydrogels were studied. Also, the cytocompatibility and osteo-differentiation potency were examined by encapsulating mesenchymal stem cells derived from adipose tissue (AMSCs) on the designed hydrogels.

Results According to the findings, our results showed an acceptable pore structure, functional groups, and degradation rate of the designed hydrogels for in vitro evaluation. In addition, employing CMC instead of CTS or adding 50% CMC to the hydrogel component could improve the hydrogel's osteo-bioactivity without the use of external osteogenic differentiation agents.

Conclusion The CMC-containing hydrogel not only caused early osteogenesis but also accelerated differentiation to the maturity phase of osteoblasts.

Keywords Carboxymethyl chitosan · Bioactivity · Hydrogel · Osteo-differentiation

Introduction

In the past decades, polymers with the ability to form gel networks great attention has been obtained to design scaffolds for tissue regeneration especially bone defects. The gelation intrinsic and architecture feature of the natural

Fereshteh Sharifi and Maryam Hassani contributed equally to this work.

✉ Shiva Irani
s.irani@srbiau.ac.ir

✉ Mohammadreza Gholami
mr.gholami@kums.ac.ir

[1] Department of Biology, Central Tehran Branch, Islamic Azad University, Tehran, Iran

[2] Hard Tissue Engineering Research Center, Tissue Engineering and Regenerative Medicine Institute, Central Tehran Branch, Islamic Azad University, Tehran, Iran

[3] Department of Biology, Science and Research Branch, Islamic Azad University, Tehran, Iran

[4] Department of Pilot Nanobiotechnology, Pasteur Institute of Iran, Tehran, Iran

[5] Department of Orthopedics, Shanghai Pudong New Area People's Hospital, Shanghai 201299, China

[6] State Key Laboratory of Oncogenes and Related Genes, Institute for Personalized Medicine, School of Biomedical Engineering, Shanghai Jiao Tong University, Shanghai 200030, China

[7] Department of Orthopedics, Shanghai Pudong Hospital, Fudan University Pudong Medical Center, Shanghai 201399, China

[8] Department of Anatomical Sciences, Medical School, Kermanshah University of Medical Sciences, Kermanshah, Iran

extracellular matrix (ECM) leads to the creation of a novel idea for presenting a functional and practical hydrogel network [1–3]. Superabsorbent biomaterials are widely believed to be water absorption and retention for producing hydrogel scaffolds. Biomaterials with natural sources like polysaccharides, polypeptides, and polynucleotides are alternative interest elements as hydrogel structure [4–7]. Because of its biocompatibility, controlled biodegradability, not induce inflammatory activity, bioresorbable nature, aqua-based solvent, suitable mechanical strength, and accessibility for modification, chitosan (CTS) is an alkaline *N*-deacetylation derivative of chitin polymer that is extensively used in biomedical specialized regeneration therapy [8–14]. Therefore, CTS and its derivatives can be considered basic hydrogel networks. Adding carboxyl and methyl groups to the CTS structure through a chemical process led to begetting carboxymethyl chitosan (CMC) derivative [15–17].

In addition, CMC exhibited various distinct characteristics over CTS, such as water solubility at natural pH, increased antibacterial and antifungal activity, and the presence of additional functional groups [18, 19]. Because CMC comprises various functional groups, such as hydroxyl and carboxyl, it may absorb water and moisture, resulting in a hydrogel with a variety of desirable features, such as high-water content, efficient biodegradation, and a natural basic source for chemical production [5, 20, 21].

The structure of CTS and CMC is a crucial consideration when employing them as parts of hydrogel networks. CTS and CMC contain monomeric building blocks that are similar to glycosaminoglycans (GAGs) in the ECM and play a functional role in cellular behavior [4]. GAGs are monomeric building blocks that correlate with collagen fibers in the ECM and play a functional role in cellular behavior. CTS has positively charged amino groups, whereas the CMC component has carboxylic groups and is negatively charged after chemical alteration. Due to their oppositely charged groups, CTS and CMC work according to the aforementioned description, the hydrogels that were developed have been utilized as therapeutic agents' scaffolds in the repair and regeneration of damaged or defective tissue. Contrary to the progress in developing hydrogels during decades, the suitable conflation of therapeutics into hydrogels to efficiently enhance bone regeneration is still challenging. In the present study, based on our previous research [8, 19, 22–24], CTS and CMC biomaterials have been used for the synthesis of the hydrogels (CTS 2%, CMC 2%, and CTS/CMC 50:50) network at room temperature, with high water content and good plasticity for inducing osteo-differentiation in AMSCs without using additional supplemental differentiator agents or growth factors [8, 22]. Initially, the structure and chemical traits of designed hydrogels (CTS, CMC, and CTS/CMC 50:50) were determined. Following that, we evaluated and compared the biocompatibility and capacity to promote osteo-differentiation of the developed hydrogels (CTS 2%, CMC 2%, and CTS/CMC 50:50) as encapsulating agents for human adipose-derived mesenchymal stem cells (AMSCs).

Materials and methods

Materials

CTS with a degree of deacetylation of 79% was purchased from Bio Basic (Canada). 3-(4,5-dimethylthiazol-2-yl)-2,5dipenyltetrazolium bromide (MTT), chloroform, 4, 6-diamidino-2-phenylindole (DAPI), and dimethyl sulfoxide (DMSO) were purchased from Sigma-Aldrich (Germany). Monochloroacetic acid, acetic acid, NaOH, formic acid, triton X-100, paraformaldehyde, sodium chloride, and ethanol were purchased from Merck (Germany). The human adipose-derived mesenchymal stem cells were obtained from the Iranian Biological Resource Center (Iran). Dulbecco's modified eagle's medium (DMEM), goat serum, fetal bovine serum (FBS), phosphate buffer saline (PBS), and trypsin/EDTA solution (0.25%) were obtained from Gibco (Canada). The anti-OSTEONECTIN primary antibody (AB13418) and the secondary antibody (AB7022) were purchased from Abcam (UK).

Preparation of hydrogels

Three stock solutions, containing CTS 2%, CMC 2%, and CTS/CMC 50:50 were prepared to construct the solution of hydrogels mentioned below.

Hydrogel CTS (2%)

The hydrogel CTS 2% (w/v) was made by dissolving 2 g of CTS powder in a 1% acetic acid–water solution overnight at room temperature with a magnetic stirrer. Under stirrer conditions, the pH of the solution was adjusted to around 6.8 by adding NaOH (10 N). The NaOH solution (0.075 N) was used to transition the sol phase to the gel phase (pH 7.2–7.4).

Hydrogel CMC (2%)

To begin, the CMC component was synthesized according to a previous study [8]. CTS powder (1 g) was dissolved in acetic acid/deionized water (DW) mixture (1/9, v/v) at room temperature overnight with continuous stirring. The CTS solution was then precipitated with sodium hydroxide. DW/isopropanol was used to wash the precipitated CTS. The filtered CTS mixture was then dissolved in isopropanol/sodium hydroxide for 5 h and stirred. After that, a combination of monochloroacetic acid and isopropanol was added dropwise and mixed continuously at room temperature for

8 h. Finally, the precipitate was filtered, washed with ethanol, and dried at room temperature in a vacuum oven (Memmert, Germany). Synthesized CMC 2% (w/v) hydrogel was prepared according to the CTS procedure.

Hydrogel CTS/CMC 50:50

To prepare hydrogel CTS/CMC 50:50, each CTS 1% (w/v) and CMC 1% (w/v) solution were separately prepared through the dissolution of CTS (1 g) and CMC (1 g) powders in acetic acid 1% in water at room temperature under continuous stirring for overnight. After that, the prepared CTS solution was added to the CMC solution. At room temperature, the final composition was homogeneously mixed with the aid of a magnetic stirrer. Under stirrer conditions, the pH of the solution was adjusted to around 6.8 by adding NaOH (10 N). The NaOH solution (pH 0.075 N) was used to transition the sol phase to the gel phase (pH 7.2–7.4). Finally, produced CTS (1%) and CMC (1%) solutions resulted in the production of a CTS/CMC (2%) hydrogel known as the CTS/CMC 50:50 hydrogel.

Scanning electron microscope (SEM)

To evaluate the hydrogels structure and pore morphology, the samples were immersed in a mixture of paraformaldehyde (2%)/ glutaraldehyde (2%) in PBS at ambition condition, removed after 1 h, washed with PBS, and frozen at – 80 ℃ followed through lyophilization (FD-5010-BT, Iran) for 24 h. The freeze-dried samples were coated with gold and observed with a scanning electron microscope (SEM, MIRA III, Czechia) at a 5 kV accelerating voltage.

Fourier transform infrared spectroscopy (FTIR)

Fourier transform infrared (FTIR) spectroscopy was used to examine the functional groups and chemical bonds that connect the CTS and CMC powders, as well as the CTS 2%, CMC 2%, and CTS/CMC 50:50 hydrogels. The FTIR spectra were collected on a Burker spectrometer (Equinox 55, Germany) with a 4 cm^{-1} resolution from 400 to 4000 cm^{-1}.

Hydrogel degradation

The degradation rates of the produced hydrogels (pH 7.2–7.4) were determined by adding 1 ml PBS to each sample. The samples were incubated at 37 °C for 0, 0.5, 1, 2, 4, 24, 48, 192, and 384 h before being sampled (n = 3 per time point). The PBS was removed and then replaced with fresh PBS every 2 days. After incubation time, the samples were taken from the PBS and placed on filter paper, and the weight loss rate was recorded. Degradation was quantified using the following equation [25]:

$$\% \text{ Degradation (t)} = \{W \text{ d } (0) - Wd(t)\}/Wd\ (0) \quad (1)$$

Where Wd (0) is the initial hydrogel mass and Wd(t) is the samples hydrogel mass at timed t.

MTT assay

Mesenchymal stem cells derived from adipose tissue (AMSCs) were cultured in a T25 tissue culture flask supplied with DMEM as the culture media containing 10% FBS at 37 ℃ in a 5% humidified atmosphere. The culture media was replaced every 2 days until passage 3. For cell seeding, an aliquot of the hydrogels (CTS 2%, CMC 2%, and CTS/CMC 50:50) was prepared to produce a homogenous solution (pH 6.8). The hydrogel samples from 100 µl of three different precursor solutions were uptake and added 5×10^5 AMSCs (cell per hydrogel). After that, NaOH solution (0.075 N) drops were added at pH 6.8 to transfer sol to gel the hydrogels containing encapsulated AMSCs (pH 7.2–7.4). For neutralizing the hydrogels containing encapsulated AMSCs were washed with PBS and DMEM. After that, the neutralized hydrogels containing encapsulated AMSCs were inserted into a 96-well tissue culture plate. After that, the media containing 10% FBS was added to each well and incubated for 1, 3, 7, and 14 days. During the evaluation period, an inverted microscope (Bell, INV-100FL) was used to check the biocompatibility of all samples. The cytotoxicity and proliferation of the hydrogels were assessed using the MTT test (n = 3 per time point) at specified intervals of time. Every two days, the culture medium was changed. Each well received a 10% MTT solution (10% total medium volume) and was incubated for 3 h. The produced formazan crystals were dissolved in DMSO, and the mixed solution's optical density (OD) at 570 nm was measured using a Bio-Tek microplate reader.

Calcium deposition on the hydrogels

The deposition of calcium on scaffolds was evaluated by calcium content assay and Alizarin Red staining. For calcium content assay, the hydrogel samples (n = 3) were washed with PBS and the deposited calcium was dissolved in HCl solution (0.6 N, Merck) via shaking in an ice bath for 1 h. The calcium concentration was measured using a calcium content kit (Pars Azmun, Iran) at 570 nm on an ELISA microplate reader. For Alizarin Red staining, the hydrogel samples were washed with PBS, fixed in a paraformaldehyde solution (10%) for 30 min, and stained by Alizarin Red solution (Sigma-Aldrich) for 45 min at room ambition. The stained samples were evaluated through optical microscopy.

Alkaline phosphatase activity assay

The bio-mineralization is one of the high-level indexes of osteo-differentiation. Alkaline phosphatase (ALP) is an important functional enzyme for guiding the initial mineralization process [26, 27]. Therefore, the determination of ALP activity can be considered an osteogenic differentiation criterion. To measure ALP activity, each hydrogel containing encapsulated AMSCs after 3, 7, and 14 days' incubation sample (n = 3) was vortexed in RIPA lysis buffer (1 ×) and Protease inhibitor (Sigma-Aldrich) for 10 s, incubated in an ice bath for 40 min and centrifuged at 15,000 rpm and 4 °C for 15 min. The absorbance of the p-nitrophenol product was measured using an ALP kit (Pars Azmun) at 405 nm on an ElISA microplate reader. The ALP values were reported as the ALP concentration normalized by the total protein concentration.

Real-time PCR

At 14 days after encapsulating AMSCs on hydrogels (CTS 2%, CMC 2%, and CTS/CMC 50:50), real-time polymerase chain reaction (PCR) was used to assess the influence of hydrogel structure on osteo-differentiation. *OSTEONECTIN* and *GAPDH* were used as osteo-differentiation markers and reference genes, respectively. To begin, total ribonucleic acid (RNA) from the encapsulated AMSCs was extracted using a whole RNA extraction kit (Pars Tous, Iran) according to the manufacturer's instructions. Then, using reverse transcriptase (RT) kit (Pars Tous, Iran) and random hexamer primers, complementary deoxyribonucleic acid (cDNA) was produced according to the manufacturer's instructions. Table 1 shows the primer sequences that were used. The PCR reactions were conducted with a 3 µl cDNA product. The annealing temperature was 95 °C for 1 min, followed by 35 cycles of 94 °C for 30 s, 60 °C for 30 s, and 72 °C for 30 s, followed by a 5-min extension time at 72 °C. Thermo-Fisher Scientific (UK) synthesis kit was utilized to perform real-time PCRs, and ABI software was used to assess the average threshold cycle. The comparative Ct technique was used to calculate gene expression levels. For this purpose, the obtained data of the target gene (*OSTEONECTIN*) and then the reference gene (*GAPDH*) were normalized and calculated. The difference in data between the tissue culture plate (TCP) control group and the CTS 2%, CMC 2%, and CTS/CMC 50:50 experimental groups was investigated. The p values of 0.05 were interpreted as being significant and the whole data are shown in the figures areas as mean ± standard error bar. All data from Real-time PCR were collected for analyzing the efficiency of reaction through REST2009 software. After determining efficiency (E), the fold change of each gene was calculated in Excel 2016 [28]. Finally, the differences between groups were analyzed using the one-way ANOVA and t-Test method and the chart of obtained results were drawn by Graph Pad Prism 9.4.1 software (USA).

$$\text{Fold change} = \left(E_{\text{target}}\right)^{\Delta ct\ \text{target(control}-\text{sample)}} \Big/ \left(E_{\text{ref}}\right)^{\Delta ct\ \text{ref(control}-\text{sample)}}$$

E_{target} = Efficiency primer for target gene; E_{ref} = Efficiency primer for the reference gene.

Immunocytochemistry (ICC) staining

After 14 days of incubation, the encapsulated AMSC into the hydrogels (CTS 2%, CMC 2%, and CTS/CMC 50:50) (n = 3) on the sterilized cover-slip placed bottom of the cell culture plate were immune-stained. The encapsulated cells were rinsed three times with PBS after being fixed in a paraformaldehyde solution in PBS (4%) and submerged in a Triton X-100 solution (4%) to improve permeability cells. Goat serum was used to prevent non-specific binding sites (10%). The fixed cells were initially incubated overnight at 4 °C with the anti-OSTEONECTIN primary antibody (1:100), washed many times with PBS, and then incubated for 1 h at room temperature with the secondary antibody (1:200). Finally, the cell nuclei were stained with DAPI solution (4′,6-diamidino-2-phenylindole) in PBS and examined with a confocal fluorescence microscope (Labomed, PCM400, Denmark) fitted with DAPI and FITC filters in darkness. The number of positive cells (defined as DAPI stained nucleus in the active cell than protein marker labeled in the cytoplasm) in each sample was adjusted by the formula presented:

Positive cells: the number of protein marker FITC/the number of nuclei DAPI labeled.

The data was analyzed through the Graph-Pad Prism version 9.4.1 (USA).

Table 1 The types and sequence of primers

Primer	Forward (5′–3′)	Reverse (3′–5′)
Primer pair *SPARC (OSTEONECTIN)*	ACATCGGGCCTTGCAAGATAC	GTTGTCTTCATCCCGCTCAT
(Reference Gene) *GAPDH*	CTCATGTCCTGGTATGACCG	CTTCCTGTTGTGCTCTTGCT

Statically analysis

The results expressed as mean ± SD are representing at least three independent experiments. The differences between groups were analyzed using the one-way ANOVA method after testing for homogeneity of variances by the PASW Statistics program package (version 19, SPSS Inc., USA). The statistical significance was assigned as *for $p \leq 0.05$, **for $p \leq 0.01$, and ***for $p \leq 0.001$.

Results

Characterization of the hydrogel's scaffolds

The SEM images of the hydrogels (CTS 2%, CMC 2%, and CTS/CMC 50:50) showed relatively stiff structure, and a linked and untangled network. Also, SEM images revealed that combining the content of CTS with CMC (50:50) in the hydrogel's component thinned the present entangled cavity wall. A combination of CTS with CMC (50:50) for producing mixed hydrogel led to alter pore size and the thinness of cavities wall hydrogel structure (Fig. 1a).

Figure 1b and c show the FTIR spectra of CTS 2%, CMC 2%, CTS/CMC 50:50 hydrogels, as well as the CTS, and CMC powders control. For the CTS control, the region of 3444 cm^{-1} was attributed to stretching vibrations of N–H and O–H bonds of amino and hydroxyl groups, respectively [29, 30]. The peak for stretching vibration of aliphatic C–H bonds, the bending vibrations of N–H bonds of amine groups, and bending vibrations of $–CH_2$ and $–CH_3$ groups appeared at 2924 cm^{-1}, 1604 cm^{-1}, and 1411 cm^{-1}, respectively [8]. The peak of 1245 cm^{-1} and 1163 cm^{-1} is related to the stretching vibration of C-N bonds of amine groups and asymmetric stretching vibration of C–O bonds of ether bridge, respectively [16, 29]. While, new alteration peaks for the synthesized CMC at 1728 cm^{-1} and 1601 cm^{-1} are related to the stretching vibration of the carbonyl (C=O) bond of carboxylic acid groups and the bending vibrations of N–H bonds of amine groups, respectively [8]. For the CMC 2% hydrogel sample, the presence of the characteristic peaks of CMC control was confirmed. All of the basic peaks related to CTS structure were observed in the CMC graph (Fig. 1b). Moreover, the peak corresponds to carboxylic at 1601 cm^{-1}, OH, and NH at 3444 cm^{-1} were amplified CTS peaks, that created and broadened peaks with high intensity. As shown in Fig. 1c, the large Decay of the OH peak at about 3100 cm^{-1} concerning C=O stretching at 1630 cm^{-1} was indicative of the successful mixing process through the amine groups on the CTS and carboxyl groups on the CMC structure [8]. Lastly, peaks decreasing at about 1090 cm^{-1} and C–H bands with the centrality of about 2880 cm^{-1} disclosed the presence of CH_3COONa made of NaOH reaction with acetic acid in all designed hydrogels (CTS 2%, CMC 2%, and CTS/CMC 50:50) (Fig. 1b) [31].

The hydrogels are submerged in PBS solution for 348 h to see how they degrade. The weight loss diagram is shown in Fig. 1c. Based on the degradation graph, all three hydrogels were gradually degraded. While CMC 2% hydrogel exhibited a more than 60% degradation rate at 384 h.

Growth and viability of the AMSCs encapsulated on the hydrogels

According to Fig. 2a and S1, there were substantial differences in the cellular proliferation rate between the different hydrogels, control, and control DF on the first day of encapsulating AMSCs on the hydrogels. While, with more time incubation, the proliferation rate of cells in CTS 2% and CTS/CMC 50:50 hydrogels became more than in CMC 2% hydrogel. However, CTS 2% hydrogels significantly promoted cell proliferation on the third day of incubation, decreasing cellular proliferation on 7 days (Fig. 2b) (**$p < 0.01$ and *** $p < 0.001$). After 14 days of AMSCs encapsulating on CTS 2%, CMC 2% hydrogels, and control DF, the proliferation cells were significantly higher than 7 days (Fig. 2b). While the encapsulated cells on CTS/CMC 50:50 hydrogel exhibited no difference in cell viability after 14 days of incubation compared with the previous time evaluation (7 days).

Osteo-inductivity of hydrogels

There was a reddish color on the hydrogels (CTS 2%, CMC 2%, and CTS/CMC 50:50) after 3 days because of the formation of calcium deposition (Fig. 3a and S2). The results showed significant differences in the calcium content for positive (control treated with external differential factor- control DF) and negative controls with the hydrogels (CTS 2%, CMC 2%, and CTS/CMC 50:50) during 14 days' incubation (**$p < 0.01$ and ***$p < 0.001$) (Fig. 3b), which revealed osteo-differentiation for the encapsulated AMSCs into the designed hydrogels. The calcium content of CMC 2% and CTS/CMC 50:50 hydrogels after 7 days of incubation was indicated significantly higher than CTS 2% hydrogels, positive and negative controls. The calcium deposition of CMC 2% hydrogel illustrated a similar trend as control DF. It is noteworthy, that the CTS/CMC 50/:50 hydrogel displayed a homological progressive process in calcium deposition until 7 days like control DF. After that, a high increment of calcium deposition of CTS/CMC 50/:50 hydrogel was observed. After 14 days incubation, the calcium content of CMC hydrogel diminished while increasing the calcium levels of CTS 2% and especially CTS/CMC 50:50 hydrogels (*** $p < 0.001$) (Fig. 3b).

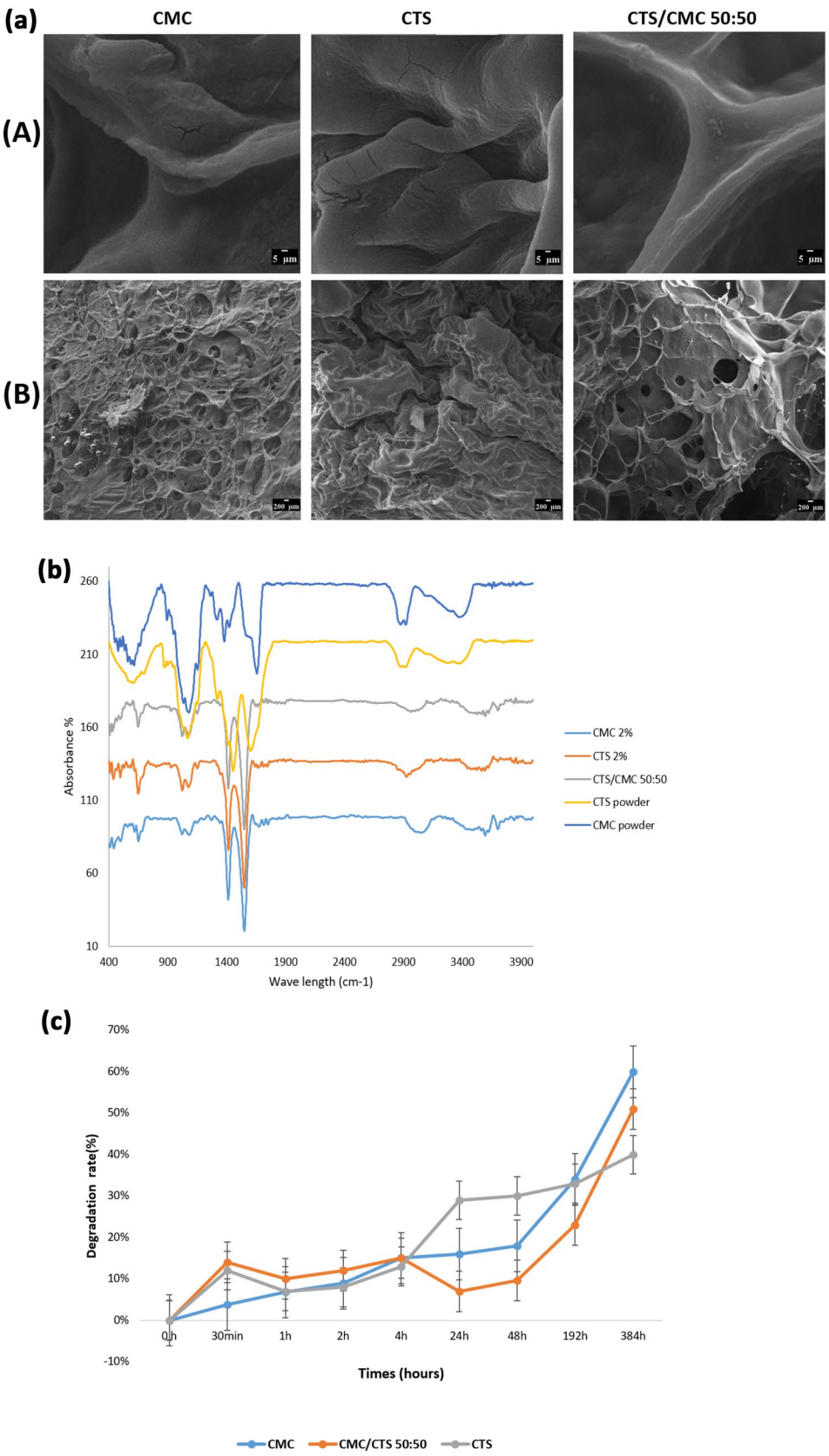

Fig. 1 **a** The scanning electron microscope (SEM) images of the morphology of the hydrogels (scale bars A: 5 µm and B: 200 µm). **b** FTIR spectra of the hydrogels. **c** FTIR spectra of the hydrogels, CTS, and CMC powder. **e** The degradation rate of the hydrogels of 0.5, 1, 2, 4, 24-, 48-, 192-, and 384-h' hydrogels drop into PBS. The results shown are means ± SD of 3 samples. Samples differing significantly from each other are indicated by vertical bars. The hydrogels refer to CTS 2%, CMC 2%, and CTS/CMC 50:50 hydrogels

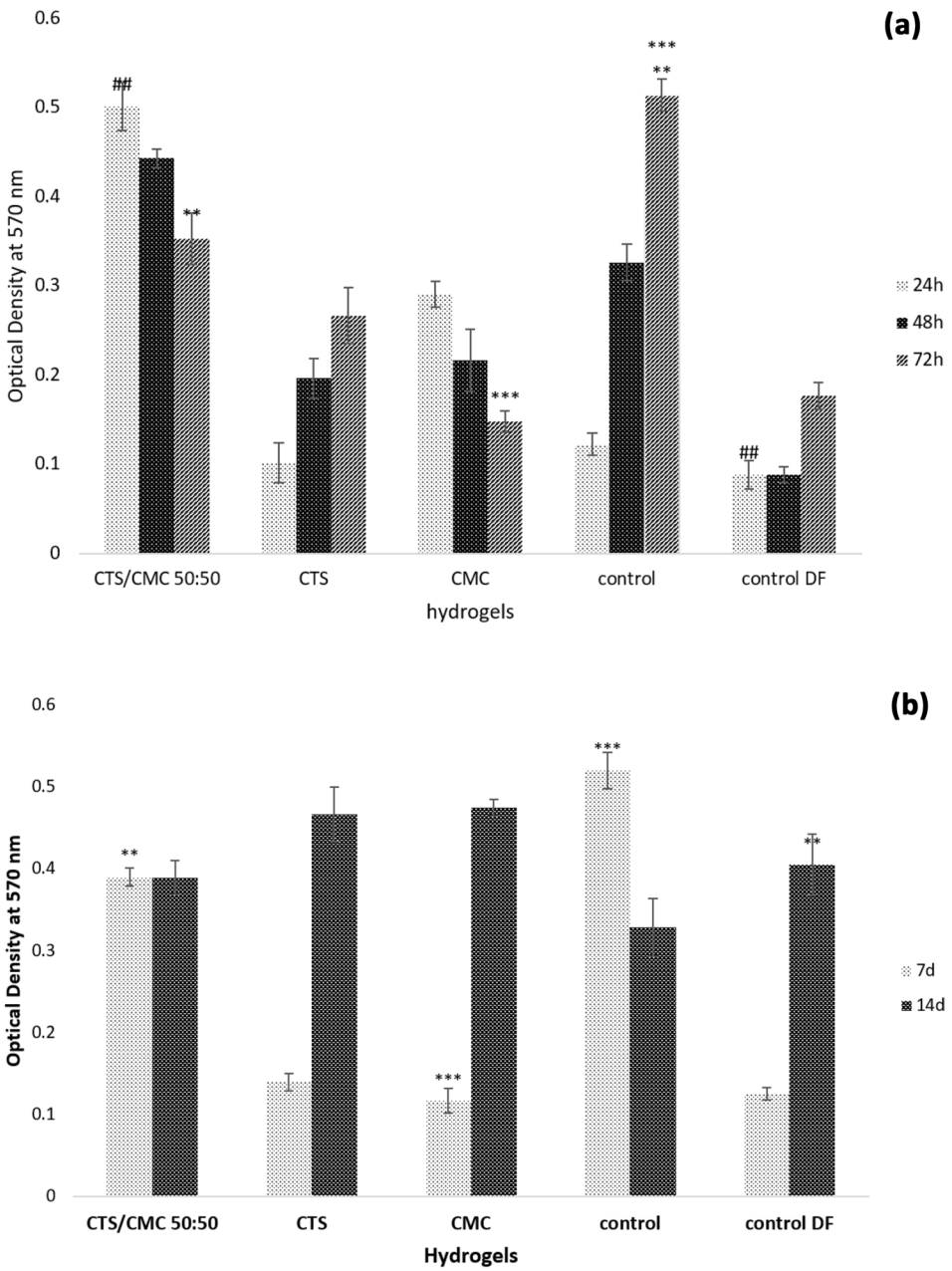

Fig. 2 The viability of encapsulated AMSCs (5×10^5 cell/hydrogel) on the hydrogels after **a**) 24 h, 48 h, and 72 h and **b**) 7 and 14 days determined using MTT assay (n = 3, **p < 0.01 and ***p < 0.001) (control DF: control supplemental differential factor)

The ALP activity of the encapsulated AMSCs was determined over 14 days without using any external osteogenic differential agent. The encapsulated cells on the hydrogels (CTS 2%, CMC 2%, and CTS/CMC 50:50) showed a considerable progress ratio in ALP activity (Fig. 4a) (*p < 0.05). In addition, the statistical comparison of ALP activity of encapsulated AMSCs on the CMC 2% hydrogel with CTS/CMC 50:50 hydrogel after 14 incubations showed a significant level of *p < 0.05.

Determining the expression of the *OSTEONECTIN* gene in encapsulated AMSCs on the hydrogels is one of the osteo-differential factors. The data revealed up-regulation of *OSTEONECTIN* for encapsulated AMSCs on the hydrogels, specifically, CTS/CMC 50:50 hydrogel (**p < 0.01 and ***p < 0.001) (Fig. 4b).

The ICC assay was done to confirm the expression of OSTEONECTIN protein for encapsulated AMSCs on the hydrogels (CTS 2%, CMC 2%, and CTS/CMC 50:50) (**p < 0.01 and *** p < 0.001) (Fig. 5a). The fluorescence microscopic images showed noticeable expression of OSTEONECTIN within a lot of several cells on the hydrogels, establishing the differentiation of encapsulated AMSCs to osteoblasts.

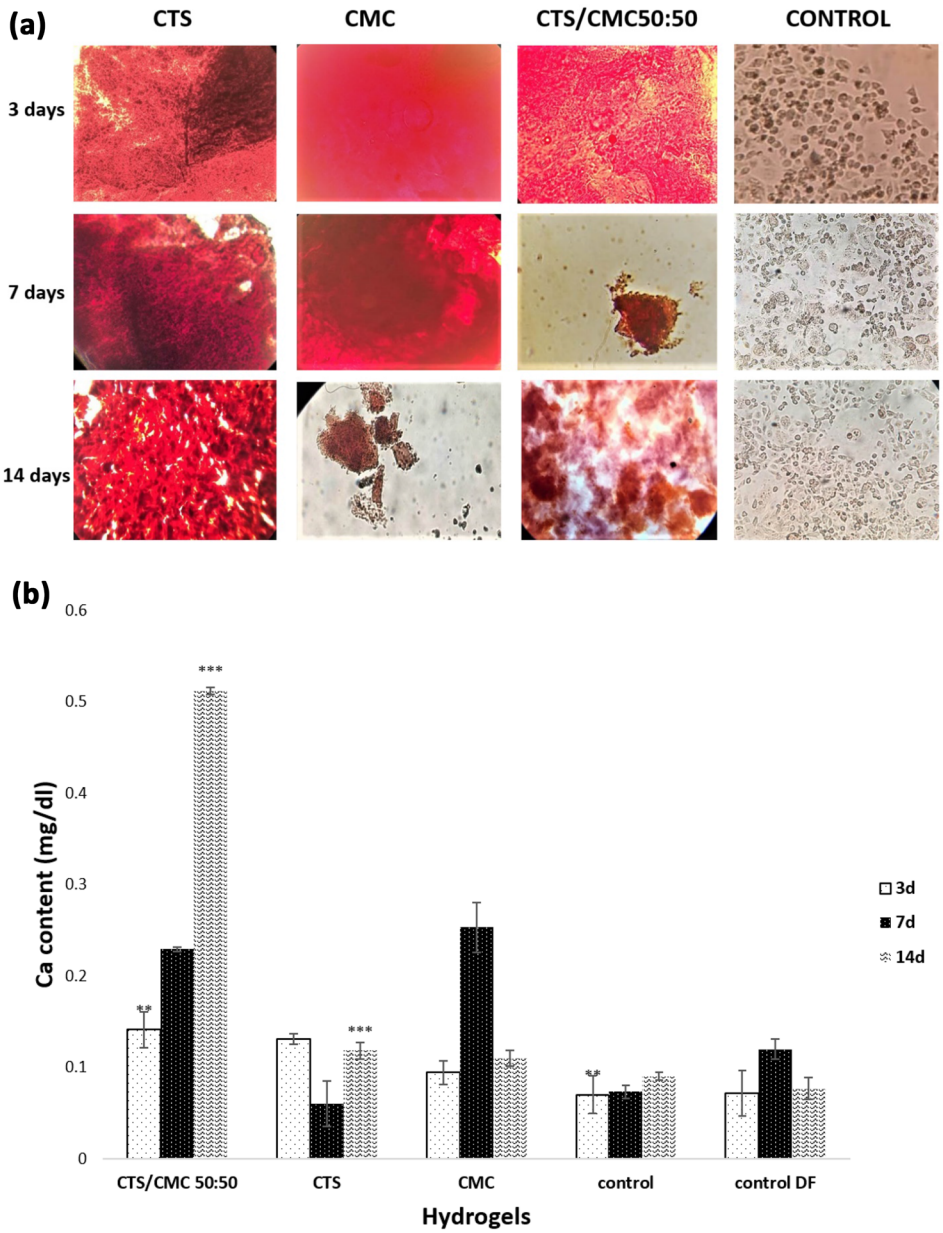

Fig. 3 **a** Alizarin red staining images of encapsulated AMSCs (5×10^5 cell/hydrogel) on the hydrogels. The magnification of images is 200. **b** Calcium content of encapsulated AMSCs (5×10^5 cell/hydrogel) on the hydrogels up to 14 days of incubation (n = 3, **p < 0.01 and ***p < 0.001) (control DF: control external differentiation factors)

Discussion

In the present research, we designed and developed CTS and its derivatives (carboxymethyl chitosan, CMC) (CTS 2%, CMC 2%, and CTS/CMC 50:50) hydrogels were utilized as hydrogel scaffolds in bone regeneration. Indeed, the chemical modification was used to improve hydrogel bioactivity by adding carboxyl and methyl groups to produce CMC as a component in the hydrogel network for preparing high similarity to the micro-environment of bone structural nature [8, 23].

The lyophilized hydrogels samples were cut and the microstructures were characterized by SEM (Fig. 1a). As shown in high-resolution SEM images, CTS/CMC 50:50 exhibited smoother and more integrated surfaces than CTS 2% and CMC 2% hydrogels (Fig. 1A). CTS polymer possesses positively charged amino groups, so these groups can be a site for creating or modifying external groups. The chemical modification of CTS led to add carboxyl and methyl groups in the backbone structure. The positively charged CTS (amine groups) and negatively charged CMC (carboxyl groups) were reacted via electrostatic interaction [17, 18]. FTIR is utilized to distinguish the bending vibrations and stretching of different functional groups, which could be used to approve the chemical structure and create new binding or functional groups of the analyzed composites [1]. According to FTIR results, all basic peaks of CTS were observed in CMC produced. Furthermore, fundamental

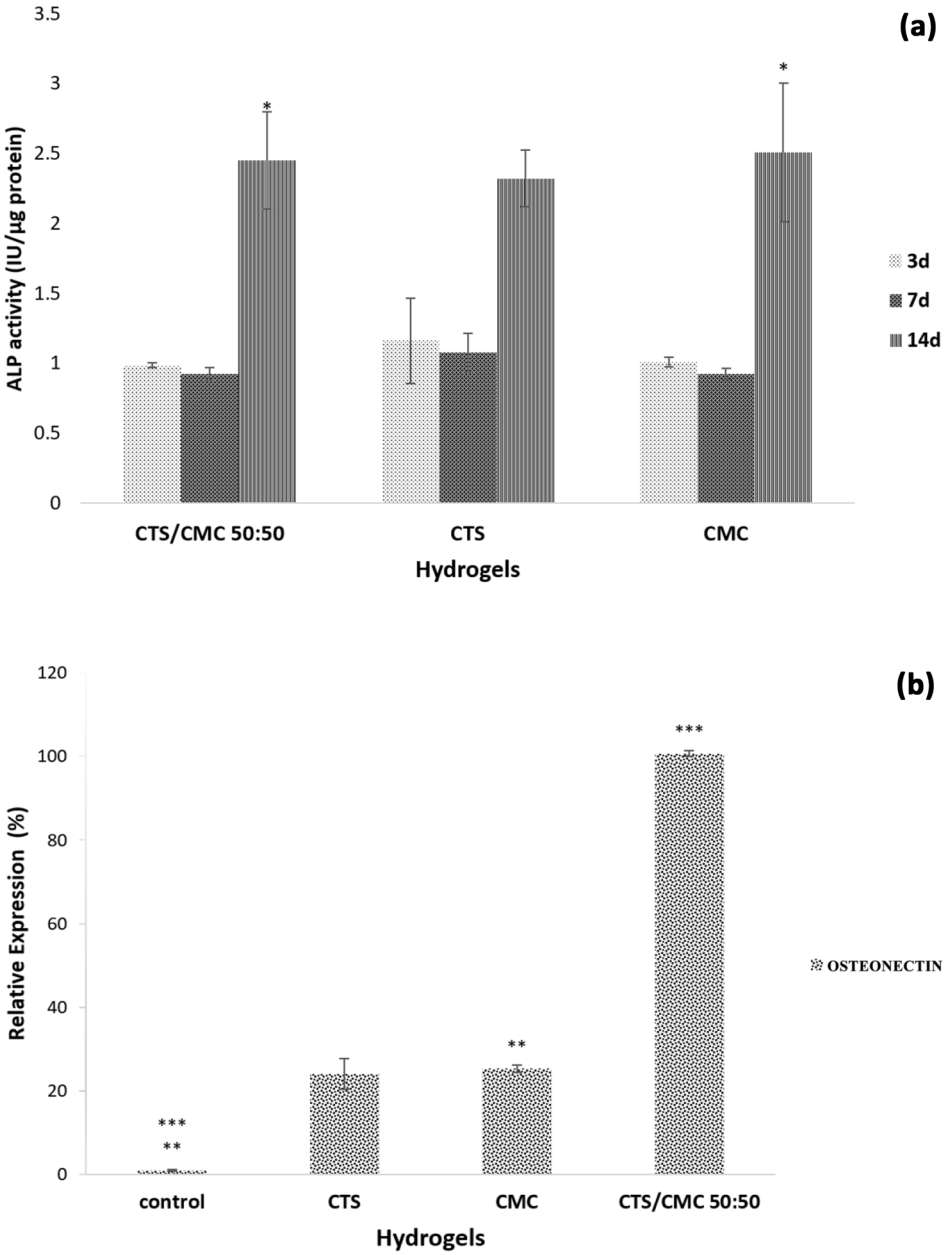

Fig. 4 **a** ALP activity of osteo-differentiated cells (5×10^5 cell/hydrogel) after 14 days incubation (n = 3, *p < 0.05). **b** Real-time PCR results for expression of *OSTEONECTIN* as osteo-differentiation marker of encapsulated AMSCs on the hydrogels (10^6 cell/ hydrogel) after 14 days (AMSCs on tissue culture plate as a control) (n = 3, **p < 0.01 and ***p < 0.001)

peaks related to functional groups of CTS and CMC were confirmed in three graphs of hydrogels (Fig. 1b). Degradation and swelling properties depend on the components and nature of the polymers utilized [32]. Due to solvent penetration and increasing swelling pressure on the polymeric network, all developed hydrogels absorbed water and lost weight in PBS. As a result of the physical pressure, the swelling ratio steadily increased, the structural strength of the ionically cross-linked hydrogels decreased, and the hydrogels in PBS collapsed. On the other hand, there was a simulated transition gel to sol phase of the hydrogels when the ambient pH was changed to 6.5 based on penetration of PBS component to the hydrogels network and ion exchange in addition to weight loss [31].

We used MTT assays to see how the chemical alteration of CTS to form CMC, as well as the combination of CTS and CMC, affected the proliferation of AMSCs. When compared to 2D cell culture in TCP, the three-dimensional (3D) network of hydrogels (CTS 2%, CMC 2%, and CTS/CMC 50:50) had a direct influence on primary cellular attachment and promoted growth during the first day (S1). The results of the first day showed that the designed hydrogels had good biocompatibility, were nontoxic, and forcefully promoted cell proliferation (Fig. 2a). Generally, diminishing proliferation is related to turn-on cellular signaling cascade during differentiation pathways [22, 33]. Increasing proliferation rate after 14 days of incubation revealed that the combination of

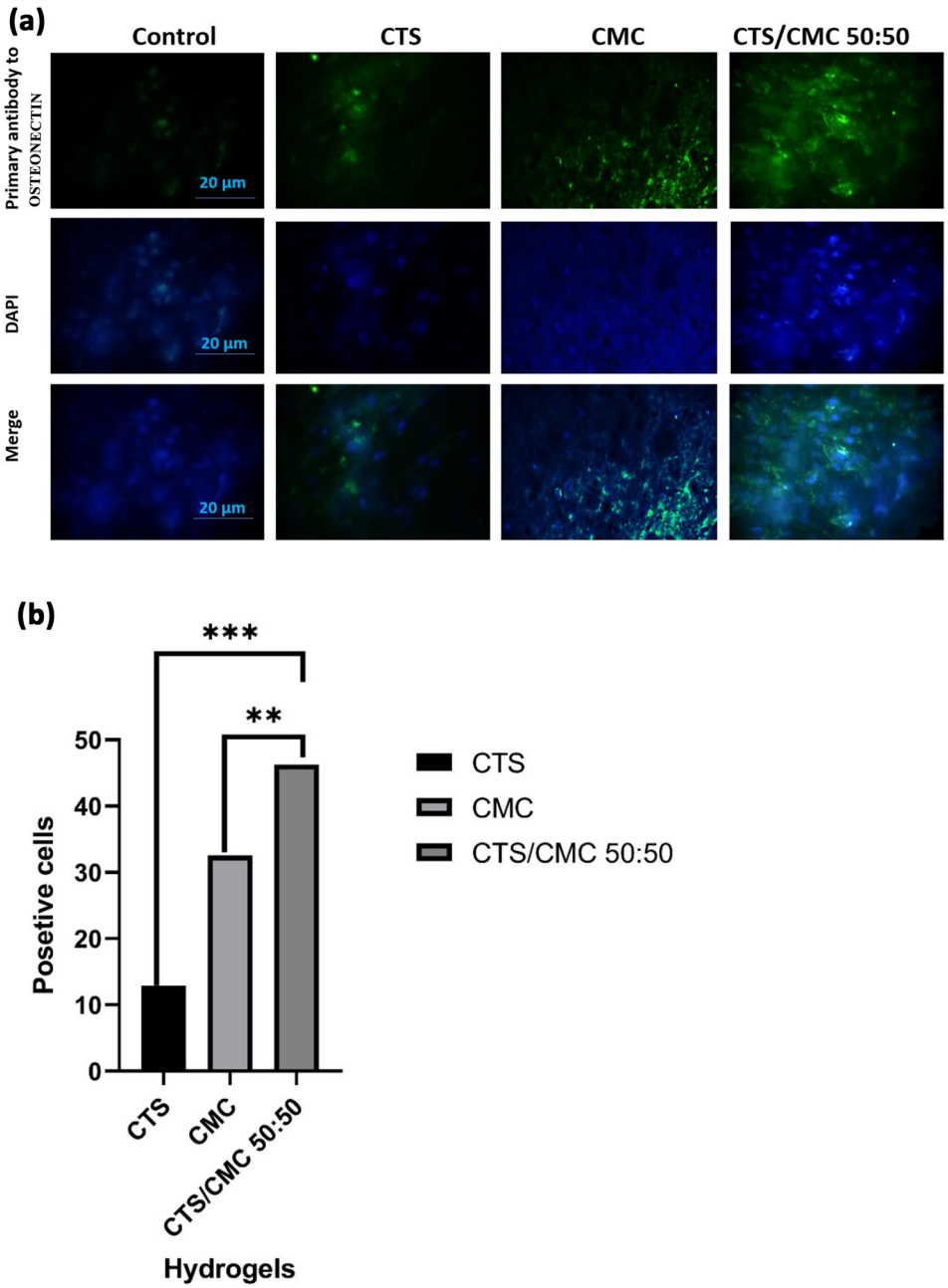

Fig. 5 **a** ICC results for expression of OSTEONECTIN of osteo-differentiated cells (5×10^5 cells/ hydrogel) after 14 days. The magnification is 20 µm. **b** The percent of osteo-differentiated encapsulated AMSCs on the hydrogels. (n = 3, **p < 0.01 and ***p < 0.001)

CMC with CTS as a bioactive component and high similarity to natural bone ECM can support cell attachment and proliferation rate besides inducing some osteogenic signaling cascades [22, 23, 34, 35]. As shown in Fig. 2a and b, CTS 2% similar to control exhibited a progressive proliferation process during 14 compared to CMC 2% and CTS/CMC 50:50 hydrogels. After 14 days of incubation, due to the preparation 3D network, CTS 2% hydrogel could support better conditions for a continuous progressive viability process than control. While the comparison of osteogenic protein markers expression between CTS 2% and other groups exhibited the CTS 2% hydrogel couldn't support osteo-differentiation similar to CMC 2% and CTS/CMC 50:50 hydrogels. Consequently, the opposite relationship between proliferation and differentiation process can be observed in CTS 2% hydrogel performance during the osteo-differentiation evaluation [21, 22, 36]. The presence of functional groups such as hydroxyl, amine, carboxyl, and more similarity to GAGs structure in the CMC prepared an acceptable situation for an attractive environment to promote proliferation levels. Therefore, the hydrogels containing the CM 2% component exhibited a high level of cellular viability than the control. Most be attention, the correlation between proliferation and

differentiation during the osteo-differentiation process in 14-day evaluation can be seen in CMC 2% and CTS/CMC 50:50 hydrogels.

The natural bone structure and composition are made of natural bio-macromolecule and hydroxyapatite elements [37, 38]. Consequently, one of the notable indexes of osteo-differentiation is bio-mineralization. Therefore, the design and preparation of bio-mimetic structure for synthesis bio-mineralization through MSCs differentiated to osteogenic without the use of external differential agents or growth factors are remaining a great challenge [39, 40]. Currently, bone tissue engineering researchers are focusing to stimulate mineralization by employing the specific material, morphology, pore size, porosity, etc. of the designed scaffold [40–42]. The calcium deposition of the encapsulated AMSCs to osteo-differentiation was qualified and quantified by Alizarin red staining and calcium content assay, respectively [23, 43]. Alizarin red staining images showed the calcium deposition with degradation rate during time evaluation. Meanwhile, the calcium content of the CMC 2% hydrogel exhibited a decreasing trend up to 14 days of incubation. While the results showed that the amount of calcium deposition on CTS/CMC 50:50 hydrogels was increased over 14 days (Figs. 3b and S2).

ALP is a glycoprotein and functions as an enzyme that adhere to the outer surface of matrix vesicles and cells [42, 44]. Many experimental studies have been established in which ALP enzymatic potential and functionality are linked to the initial bio-mineralization process [26, 27]. Roberts et al. and Kim et al. studies showed that the removal of ALP substrate from in vitro environment led to prevent calcification of cultured bone cells [45, 46]. Indeed, ALP enhanced extracellular mineralization through the release of inorganic phosphate from the bio-mineralization inhibitor inorganic pyrophosphate. The hydroxyapatite formation is initiated using the agglomeration of calcium and inorganic phosphate, followed through crystal extension, mainly in the creation of hydroxyapatite crystal [42, 47, 48]. For this purpose, ALP activity was measured as an enzyme involved in the mineralization of bone in the AMSCs encapsulated into designed hydrogels. The hydrogels containing CMC could promote the osteo-differentiation process and increment the ALP expression after 14 incubation [22, 36, 49–51]. With respect to bone tissue engineering, the affinity for biologically active proteins such as ALP and the effect of utilizing structure as a scaffold with suitable components and a rougher surface could be stimulating the formation of the natural healing processes of the surrounding bone. And the other hand, there is the opposite correlation between ALP expression and calcium deposition/content [50–52]. As shown in Fig. 3b and 4a, the increasing ALP gene expression and protein activity led to a decrease the calcium deposition. The data displayed that encapsulated AMSCs were differentiated to mature osteoblasts, therefore the potency of the hydrogels network to enhance the stem cells down the osteogenesis pathway.

Evaluating the osteoinductive potential of the hydrogels was done by ALP activity, real-time PCR, and immunocytochemistry (ICC) assay. The ALP expression and activity mostly happen before the mineralization process, so it can be considered an early osteogenesis marker [53, 54]. The ALP data showed that designed hydrogels specific CMC 2% hydrogel could induce ALP activity without using any external osteogenic differential agents during 14 days' incubation. Another factor to check the osteogenesis differentiation of encapsulated AMSCs on the hydrogels (CTS 2%, CMC 2%, and CTS/CMC 50:50) was quantitatively measuring the expression of OSTEONECTIN in mRNA levels by real-time PCR after 14 days. OSTEONECTIN mRNA is highly expressed at the initiation of the osteo-differentiation process, while its expression declines as the mature osteoblasts [23]. Evaluating mRNA expression must be confirmed by protein synthesis and activity, due to the post-transcriptional regulation of the genes, and protein modification can be a side effect on protein production and function [22, 36]. Consequently, after determining OSTEONECTIN mRNA expression and ALP activity as osteo-differentiation markers, the ICC assay was carried out for confirming the expression of OSTEONECTIN protein as osteo-differential protein in encapsulated AMSCs on the (CTS 2%, CMC 2%, and CTS/CMC 50:50) hydrogels (Figs. 5a and S3). The higher expression (46.27) for the encapsulated AMSCs on the CTS/CMC 50:50 hydrogels confirmed the function of CMC as an effective bioactive component and prepared a high mimic environment structure to the functional bone for inducing osteogenesis differentiation (Fig. 5b) [55]. While most tissue engineering research must be used supplemental media or growth factors to induce osteogenic differentiation [21, 52, 56–58]. The in-vitro evaluation results showed the employment of CMC on the hydrogel structure can stimulate the osteogenesis process in AMSCs without using any osteogenic differential agents or growth factors.

Conclusions

The design and development of new hydrogel-based natural biomaterials with bioactivity properties are essential for the progress of applications related to osteo-tissue regeneration. Here, we report osteo-differentiation promoted through hydrogels (CTS 2%, CMC 2%, and CTS/CMC 50:50) structure without using external osteo-differentiation agents. Prepared hydrogels based on the positively charged natural polymer CTS, negatively charged CMC, and combination of CTS with CMC led to the formation of hydrogels with porous network and functional groups, as shown using scanning electron microscopy (SEM) and Fourier transform

infrared spectroscopy (FTIR). The effect of utilizing CMC and the combination of CMC with CTS as a component of hydrogels in the degradation and swelling rate were determined during 384 h. Also, our results exhibited that the designed hydrogels were cytocompatible, and applying CMC in hydrogel structure could promote the osteo-differentiation of encapsulated mesenchymal stem cells derived from adipose tissue (AMSCs) in vitro conditions. Eventually, developing hydrogel structure by chemical modification on the natural polymer can enhance bioactivity and suggest a new strategy for producing a three-dimensional network as substrate in tissue regeneration applications in the future.

Supplementary Information The online version contains supplementary material available at https://doi.org/10.1007/s11033-022-08013-9.

Funding This research received no external funding.

Data availability They are available on the request.

Declarations

Conflict of interest The authors declare no competing interest.

References:

1. Fares MM, Sani ES, Lara RP, Oliveira RB, Khademhosseini A, Annabi N (2018) Interpenetrating network gelatin methacryloyl (GelMA) and pectin-g-PCL hydrogels with tunable properties for tissue engineering. Biomater Sci 6(11):2938–2950
2. Chang S, Liu Z, Wang X (2022) Advances of stimulus-responsive hydrogels for bone defects repair in tissue engineering. Gels 8:389
3. Ghalei S, Handa H (2021) Nitric oxide-releasing gelatin methacryloyl/silk fibroin interpenetrating polymer network hydrogels for tissue engineering applications. ACS Biomater Sci Eng 8(1):273–283
4. Zou Z, Wang L, Zhou Z, Sun Q, Liu D, Chen Y, Zou X et al (2021) Simultaneous incorporation of PTH (1–34) and nano-hydroxyapatite into chitosan/alginate hydrogels for efficient bone regeneration. Bioactive Mater 6(6):1839–1851
5. Nie J, Pei B, Wang Z, Hu Q (2019) Construction of ordered structure in polysaccharide hydrogel: a review. Carbohydr Polym 205:225–235
6. Nie H, Liu M, Zhan F, Guo M (2004) Factors on the preparation of carboxymethylcellulose hydrogel and its degradation behavior in soil. Carbohydr Polym 58(2):185–189
7. Dutta SD, Hexiu J, Patel DK, Ganguly K, Lim KT (2021) 3D-printed bioactive and biodegradable hydrogel scaffolds of alginate/gelatin/cellulose nanocrystals for tissue engineering. Int J Biol Macromol 167:644–658
8. Sharifi F et al (2018) Polycaprolactone/carboxymethyl chitosan nanofibrous scaffolds for bone tissue engineering application. Int J Biol Macromol 115:243–248
9. Tang Y, Du Y, Li Y, Wang X, Hu X (2009) A thermosensitive chitosan/poly (vinyl alcohol) hydrogel containing hydroxyapatite for protein delivery. J Biomed Mater Res Part A 91(4):953–963
10. Anitha A, Sowmya S, Kumar PS, Deepthi S, Chennazhi KP, Ehrlich H, Jayakumar R et al (2014) Chitin and chitosan in selected biomedical applications. Progr Polym Sci 39(9):1644–1667
11. Qi L, Xu Z, Jiang X, Hu C, Zou X (2004) Preparation and antibacterial activity of chitosan nanoparticles. Carbohydr Res 339(16):2693–2700
12. No HK, Park NY, Lee SH, Meyers SP (2002) Antibacterial activity of chitosans and chitosan oligomers with different molecular weights. Int J Food Microbiol 74(1–2):65–72
13. Li Q, Dunn ET, Grandmaison EW, Goosen MF (2020) Applications and properties of chitosan. In: Goosen MFA (ed) Applications of chitin and chitosan. Boca Raton, CRC Press, pp 3–29
14. Tsai GJ, Su WH (1999) Antibacterial activity of shrimp chitosan against *Escherichia coli*. J Food Prot 62(3):239–243
15. Hunt JA, Chen R, van Veen T, Bryan N (2014) Hydrogels for tissue engineering and regenerative medicine. J Mater Chem B 2(33):5319–5338
16. Ji X, Yang W, Wang T, Mao C, Guo L, Xiao J, He N (2013) Coaxially electrospun core/shell structured poly (L-lactide) acid/chitosan nanofibers for potential drug carrier in tissue engineering. J Biomed Nanotechnol 9(10):1672–1678
17. Wu T, Huang J, Jiang Y, Hu Y, Ye X, Liu D, Chen J (2018) Formation of hydrogels based on chitosan/alginate for the delivery of lysozyme and their antibacterial activity. Food Chem 240:361–369
18. Zhong QK, Wu ZY, Qin YQ, Hu Z, Li SD, Yang ZM, Li PW (2019) Preparation and properties of carboxymethyl chitosan/alginate/tranexamic acid composite films. Membranes 9(1):11
19. Alemi PS et al (2019) Synergistic effect of pressure cold atmospheric plasma and carboxymethyl chitosan to mesenchymal stem cell differentiation on PCL/CMC nanofibers for cartilage tissue engineering. Polym Adv Technol 30:1356
20. Wach RA, Mitomo H, Yoshii F, Kumo T (2001) Hydrogel of biodegradation cellulose derivatives. II. Effect of some factors on radation-induced crosslinking of CMC. J Appl Polym Sci 81:3000–3017
21. Tao F, Cheng Y, Tao H, Jin L, Wan Z, Dai F, Deng H et al (2020) Carboxymethyl chitosan/sodium alginate-based micron-fibers fabricated by emulsion electrospinning for periosteal tissue engineering. Mater Design 194:108849
22. Sharifi F, Atyabi SM, Irani S, Bakhshi H (2020) Bone morphogenic protein-2 immobilization by cold atmospheric plasma to enhance the osteoinductivity of carboxymethyl chitosan-based nanofibers. Carbohydr Polym 231:115681
23. Arab-Ahmadi S, Irani S, Bakhshi H, Atyabi F, Ghalandari B (2021) Immobilization of carboxymethyl chitosan/laponite on polycaprolactone nanofibers as osteoinductive bone scaffolds. Polym Adv Technol 32(2):755–765
24. Arab-Ahmadi S, Irani S, Bakhshi H, Atyabi F, Ghalandari B (2021) Immobilization of cobalt-loaded laponite/carboxymethyl chitosan on polycaprolactone nanofiber for improving osteogenesis and angiogenesis activities. Polym Adv Technol 32:4362
25. Gupta D, Tator CH, Shoichet MS (2006) Fast-gelling injectable blend of hyaluronan and methylcellulose for intrathecal, localized delivery to the injured spinal cord. Biomaterials 27(11):2370–2379
26. Anderson HC (1995) Molecular biology of matrix vesicles. Clin Orthop Relat Res 314:266–280
27. Zhong C, Chu CC (2012) Biomimetic mineralization of acid polysaccharide-based hydrogels: towards porous 3-dimensional bone-like biocomposites. J Mater Chem B 22(13):6080–6087
28. Pfaffl MW (2001) A new mathematical model for relative quantification in real-time RT–PCR. Nucleic Acids Res 29(9):45
29. Mohammadnezhad J, Bakhshi H et al (2016) Preparation and evaluation of chitosan-coated eggshell particles as copper(II) biosorbent. Desalin Water Treatment 57:1693–1704
30. Ray M, Anis A, Banthia AK (2010) Development and characterization of chitosan based polymeric hydrogel membranes. Des Monomers Polym 13:193–206

31. Hassani F, Ebrahimi B, Moini A, Ghiaseddin A, Bazrafkan M, Hassanzadeh G, Valojerdi MR (2020) Chitosan hydrogel supports integrity of ovarian follicles during in vitro culture: a preliminary of a novel biomaterial for three dimensional culture of ovarian follicles. Cell J (Yakhteh) 21(4):193
32. Yar M, Gigliobianco G, Shahzadi L, Dew L, Siddiqi SA, Khan AF, MacNeil S et al (2016) Production of chitosan PVA PCL hydrogels to bind heparin and induce angiogenesis. Int J Polym Mater Polym Biomater 65(9):466–476
33. Sharifi F, Irani S, Azadegan G, Pezeshki-Modaress M, Zandi M, Saeed M (2020) Co-electrospun gelatin-chondroitin sulfate/polycaprolactone nanofibrous scaffolds for cartilage tissue engineering. Bioactive Carbohydr Dietary Fibre 22:100215
34. Rusdianto Budiraharjo KGN (2012) Hydroxyapatite-coated carboxymethyl chitosan scaffolds for promoting osteoblast and stem cell differentiation. J Colloid Interface Sci 366:224–232
35. Upadhyaya L, Agarwal V, Tewari RP (2014) The im plications of recent advances in carboxym eth yl chitosan based targeted drug delivery an d tissu e engin eering applicat ions. J Controlled Release 186:54–87
36. Neuss S et al (2008) Assessment of stem cell/biomaterial combinations for stem cell-based tissue engineering. Biomaterials 29(3):302–313
37. Siddiqui N, Jabbari E (2015) Osteogenic differentiation of human mesenchymal stem cells in freeze-gelled chitosan/nano β-tricalcium phosphate porous scaffolds crosslinked with genipin. Mater Sci Eng C 54:76–83
38. Zaharia A, Muşat V, Anghel EM, Atkinson I, Mocioiu OC, Buşilă M, Pleşcan VG (2017) Biomimetic chitosan-hydroxyapatite hybrid biocoatings for enamel remineralization. Ceram Int 43:11390–11402
39. Salama A (2018) Chitosan based hydrogel assisted spongelike calcium phosphate mineralization for in-vitro BSA release. Int J Biol Macromol 108:471–476
40. Liang H, Sheng F, Zhou B, Pei Y, Li B, Li J (2017) Phosphoprotein/chitosan electrospun nanofibrous scaffold for biomineralization. Int J Biol Macromol 102:218–224
41. Douglas TE, Skwarczynska A, Modrzejewska Z, Balcaen L, Schaubroeck D, Lycke S, Leeuwenburgh SC (2013) Acceleration of gelation and promotion of mineralization of chitosan hydrogels by alkaline phosphatase. Int J Biol Macromol 56:122–132
42. Li N, Zhou L, Xie W, Zeng D, Cai D, Wang H, Li L et al (2019) Alkaline phosphatase enzyme-induced biomineralization of chitosan scaffolds with enhanced osteogenesis for bone tissue engineering. Chem Eng J 371:618–630
43. Orafa Z, Irani S, Zamanian A, Bakhshi H, Nikukar H, Ghalandari B (2021) Evaluation of biocompatibility of PLA scaffold coated with laponite on human bone marrow mesenchymal stem cells. J Anim Biol 13(4):101–117
44. Fu C, Yang X, Tan S, Song L (2017) Enhancing cell proliferation and osteogenic differentiation of MC3T3-E1 pre-osteoblasts by BMP-2 delivery in graphene oxide-incorporated PLGA/HA biodegradable microcarriers. Sci Rep 7(1):1–13
45. Kim JA, Yun HS, Choi YA, Kim JE, Choi SY, Kwon TG, Park EK (2018) Magnesium phosphate ceramics incorporating a novel indene compound promote osteoblast differentiation in vitro and bone regeneration in vivo. Biomaterials 157:51–61
46. Roberts S, Narisawa S, Harmey D, Millán JL, Farquharson C (2007) Functional involvement of PHOSPHO1 in matrix vesicle–mediated skeletal mineralization. J Bone Miner Res 22(4):617–627
47. Rader BA (2017) Alkaline phosphatase, an unconventional immune protein. Front Immunol. https://doi.org/10.3389/fimmu.2017.00897
48. Favarin BZ, Andrade MAR, Bolean M, Simão AMS, Ramos AP, Hoylaerts MF, Millán JL, Ciancaglini P (2017) Effect of the presence of cholesterol in the interfacial microenvironment on the modulation of the alkaline phosphatase activity during in vitro mineralization. Colloids Surf B 155:466–476
49. Khorasani MT, Joorabloo A, Moghaddam A, Shamsi H, MansooriMoghadam Z (2018) Incorporation of ZnO nanoparticles into heparinised polyvinyl alcohol/chitosan hydrogels for wound dressing application. Int J Biol Macromol 114:1203–1215
50. Domingos M, Gloria A, Gristina R, Ambrosio L, Bártolo PJ, Favia P, Uovo F, Gloria A, Gristina R, Ambrosio L, Bártolo PJ, Favia P (2013) Improved osteoblast cell affinity on plasma-modified 3-D extruded PCL scaffolds. Acta Biomater 9(4):5997–6005
51. Marolt D, Vunjak-Novakovic G (2010) Bone tissue engineering with human stem cells. Stem Cell Res Therapy. 1(2):10
52. Moghadam FH, Dehghan M, Eslami G, Nadri H, Moradi A, Vahedian-Ardakani H, Barzegar K (2014) Differentiation of bone marrow mesenchymal stem cells into chondrocytes after short term culture in alkaline medium. Int J Hematol-Oncol Stem Cell Res 8(4):12
53. Birmingham E, Niebur G, McHugh P (2012) Osteogenic differentiation of mesenchymal stem cells is regulated by osteocyte and osteoblast cells in a simplified bone niche. Eur Cell Mater 23:13–27
54. Shi Z, Neoh K, Kang E, Poh CK, Wang W (2009) Surface functionalization of titanium with carboxymethyl chitosan and immobilized bone morphogenetic protein-2 for enhanced osseointegration. Biomacromol 10:1603–1611
55. Baratta JL, Ngo A, Lopez B, Kasabwalla N, Longmuir KJ, Robertson RT (2009) Cellular organization of normal mouse liver: a histological, quantitative immunocytochemical, and fine structural analysis. Histochem Cell Biol 131(6):713–726
56. Anne Neumann AC (2013) BMP2-loaded nanoporous silica nanoparticles promote osteogenic differentiation of human mesenchymal stem cells. RSC Adv 3:24222–24230
57. Gamblin A-L et al (2014) Bone tissue formation with human mesenchymal stem cells and biphasic calcium phosphate ceramics: the local implication of osteoclasts and macrophages. Biomaterials 35(36):9660–9667
58. Kilmer CE, Battistoni CM, Cox A, Breur GJ, Panitch A, Liu JC (2020) Collagen type I and II blend hydrogel with autologous mesenchymal stem cells as a scaffold for articular cartilage defect repair. ACS Biomater Sci Eng 6(6):3464–3476